

# 1 Laplace transform analytic element method for transient porous media 2 flow

3 Kristopher L. Kuhlman and Shlomo P. Neuman

4 *Department of Hydrology and Water Resources*

5 *University of Arizona, Tucson, AZ 85721*

6 **Abstract.** A unified theory of the Laplace transform analytic element method (LT-AEM) for solving transient  
7 porous media flow problems is presented. LT-AEM applies the analytic element method (AEM) to the modified  
8 Helmholtz equation, the Laplace-transformed diffusion equation. LT-AEM uses superposition and boundary  
9 collocation with Laplace-space convolution to compute flexible semi-analytic solutions from a small collection  
10 of fundamental elements. The elements discussed are derived using eigenfunction expansions of element shapes in  
11 their natural coordinates. A new formulation for a constant strength line source is presented in terms of elliptical  
12 coordinates and complex-parameter Mathieu functions. Examples are given illustrating how leaky and damped  
13 wave hydrologic problems can be solved with little modification using existing LT-AEM techniques.

14 **Keywords:** analytic element, Laplace transform, diffusion equation, modified Helmholtz equation, elliptical  
15 coordinates, transient line source, Mathieu functions

16 **Abbreviations:** AEM – analytic element method; LT-AEM – Laplace transform analytic element method

17

## 1. Introduction

18 The analytic element method (AEM) provides semi-analytic solutions to linear porous media  
19 flow problems through superposition of fundamental solutions. The original development of  
20 AEM is due to Strack and his co-workers at the University of Minnesota [1]. During its initial  
21 development, it was compared to the boundary element method [2], but the eigenfunction  
22 expansion approach discussed here may be considered a special case of the spectral method (see  
23 [3, Sect. 3.1] and [4, App. C]). Each AEM element satisfies the governing equation, while spectral  
24 elements typically do not. The majority of AEM applications to date have been concerned  
25 with vertically-averaged steady-state groundwater flow (the two-dimensional (2D) Laplace and  
26 Poisson equations in the horizontal plane). AEM has been extended to three-dimensional [5],  
27 transient [6], multi-layer [7], and linearized unsaturated [8] flow problems. Review papers [9–11]  
28 and textbooks by Strack [12] and Haitjema [13] cover the fundamentals, discuss applications,  
29 and mention some recent advances.

30 AEM partially fills a gap between analytic solutions derived for simple geometries (e.g.,  
31 radially-symmetric flow to a well) and distributed-parameter gridded models (e.g., finite element  
32 methods). AEM is well-suited for time-independent boundary value problems; applications to  
33 transient diffusion have proceeded in several directions.

34 The earliest extension of AEM to transient flow [14] was discontinuous in time, using a grid to  
35 simulate transient storage. The corresponding space discretization offset the mesh-free benefit  
36 normally associated with AEM. Another early approach [15] combined steady and transient  
37 elements, using line and area sources to model transient effects; transient storage effects were  
38 assumed piecewise-constant in time and the method required zero net withdrawal of water from  
39 the aquifer. While not an AEM solution, Butler and Liu [16] developed a solution for transient  
40 flow to a well in the presence of a single circular inhomogeneity, using an approach similar to  
41 that taken here. Bakker [17] used a temporal Fourier transform to apply the AEM to problems  
42 comprised of a finite number of temporal harmonics. Strack [18] described a general AEM  
43 approach in which localized transient perturbation elements are superimposed on a confined  
44 steady background that uses finite differences in time.

45 Furman and Neuman [6] first used AEM to solve the Laplace-transformed diffusion equa-  
46 tion. LT-AEM numerically back-transforms the solution into the time domain using an inverse



47 Laplace transform algorithm. In contrast to the Fourier transform approach, the use of the  
 48 Laplace transform obviates the need for periodicity and can incorporate initial conditions.  
 49 We illustrate LT-AEM elements constructed using eigenfunction expansion and Laplace-space  
 50 convolution. Steady-state multi-layer aquifer systems [7] and linearized steady unsaturated flow  
 51 [19, 20] also lead to the Helmholtz equation. We show how these type of homogeneous distributed  
 52 sources can be incorporated into the LT-AEM. The elements outlined here are restricted to  
 53 simple geometries (i.e., circles and ellipses), but other techniques (e.g., those utilized in spectral  
 54 element modeling [3, Chap. 17]) can be used to extend LT-AEM to more general geometries.

## 55 2. Laplace Transform AEM

56 Hydraulic head in a transient, 2D, confined, elastic aquifer is described by the diffusion equation,

$$Kb\nabla^2 h(\mathbf{x}, t) + bG = bS_s \frac{\partial h(\mathbf{x}, t)}{\partial t}; \quad (1)$$

57 where  $h(\mathbf{x}, t)$  is vertically-averaged hydraulic head [ $L$ ],  $b$  is aquifer thickness [ $L$ ],  $G$  is a volumetric  
 58 source term [ $1/T$ ],  $K$  is the hydraulic conductivity [ $L/T$ ], and  $S_s$  is specific storage [ $1/L$ ].  $K$   
 59 is assumed isotropic; both  $K$  and  $S_s$  are assumed homogeneous. For horizontal 2D flow, a unit  
 60 aquifer thickness is assumed for simplicity (unless stated otherwise), without loss of generality.  
 61 2D vertical-plane flow could also be simulated with this approach, e.g., flow under a wide dam  
 62 on a permeable foundation.

63 In AEM it is standard to work with discharge potential [ $L^3/T$ ],  $\Phi = bKh + C$ , where  $C$  is an  
 64 arbitrary reference [12] that we conveniently set to zero. Applying the Laplace transform [21,  
 65 Chap. 4] to (1), written in terms of  $\Phi$ , with  $G = 0$ , gives

$$\alpha \nabla^2 \bar{\Phi}(\mathbf{x}) = \bar{\Phi}(\mathbf{x})p - \Phi_0, \quad (2)$$

66 where  $\alpha = K/S_s$  is hydraulic diffusivity [ $L^2/T$ ],  $p$  is the Laplace transform parameter [ $T^{-1}$ ],  
 67  $\bar{\Phi}(\mathbf{x})$  is the transformed discharge potential [ $L^3$ ], and  $\Phi_0$  is the initial value of  $\Phi$ . To render (2)  
 68 homogeneous we set  $\Phi_0 = 0$ ; non-zero initial conditions are introduced using impulse area  
 69 sources at  $t = 0$  [22]. The governing equation in Laplace space is the Yukawa [23] or modified  
 70 Helmholtz equation

$$\nabla^2 \bar{\Phi}(\mathbf{x}) - \kappa^2 \bar{\Phi}(\mathbf{x}) = 0, \quad (3)$$

71 where  $\kappa^2 = p/\alpha$  [ $L^{-2}$ ] is analogous to the wave number in wave propagation problems [24, Sect.  
 72 1.1.2], or alternatively  $\kappa = 1/(Z_0 K)$ , where  $Z_0$  is the mechanical analog of impedance [25, Chap.  
 73 7].

### 74 2.1. LAPLACE-SPACE CONVOLUTION

75 Duhamel's theorem [26, Chap. 5] states that temporal behavior of a function can be obtained  
 76 from convolution of the impulse response,  $\Phi_{\text{imp}}(\mathbf{x}, t)$ , and a time behavior,  $g(t)$ , through the  
 77 convolution integral

$$\Phi_{\text{gen}}(\mathbf{x}, t) = \int_0^t \Phi_{\text{imp}}(\mathbf{x}, t - \tau) g(\tau) d\tau. \quad (4)$$

78 LT-AEM elements are derived in Laplace space where (4) becomes

$$\bar{\Phi}_{\text{gen}}(\mathbf{x}, p) = \bar{\Phi}_{\text{imp}}(\mathbf{x}, p) \bar{g}(p). \quad (5)$$

79 When convolution is performed in the time domain [15], each different time behavior (e.g.,  
 80 constant, pulse, or linearly-increasing in time) requires approximation of (4). LT-AEM allows for  
 81 separate handling of the time ( $\bar{g}$ ) and space ( $\bar{\Phi}_{\text{imp}}$ ) behavior of elements through the numerical  
 82 inverse Laplace transform.

83 Many useful  $\bar{g}(p)$  functions can be found tabulated in the literature (e.g., [27, Chap. 29], [21,  
 84 App. A], and [26, Sect. 7.3]); piecewise linear or constant functions can be used to describe fairly  
 85 general behavior. While it would be possible to perform the convolution in the time domain, we  
 86 expect that this increases the required effort. The time-domain convolution integral (4) requires  
 87 integrating  $0 \leq \tau \leq t$ , essentially equivalent to time-marching required by an initial value  
 88 problem (e.g., explicit finite differences in time).

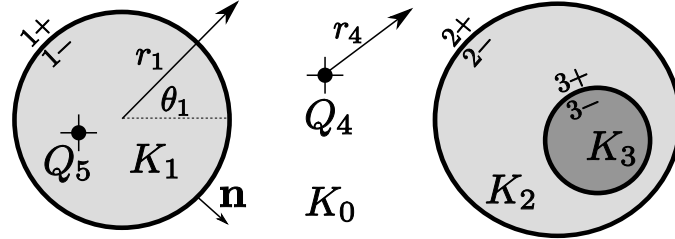


Figure 1. Example with 3 circular elements with different  $K$  (background  $K_0$ ) and 2 prescribed point sources,  $Q_4$  and  $Q_5$ .

## 89 2.2. BOUNDARY MATCHING

90 Elements are mathematical entities that represent physical objects in the flow system. AEM  
 91 and LT-AEM use non-intersecting elements to represent areas of differing properties and source  
 92 terms (see Figure 1), by enforcing head and normal flux continuity along the element boundaries.  
 93 Each LT-AEM element is derived with implied zero initial condition and zero effect at large  
 94 distance. The elements in Figure 1 will be used as an example, 2 point sources of prescribed  
 95 strength and 3 circular regions of different  $K$  with unknown strengths. Head matching consists  
 96 of setting

$$\bar{h}_{\text{tot}}^+(r_{n0}) = \bar{h}_{\text{tot}}^-(r_{n0}); \quad (6)$$

97 the total head,  $\bar{h}_{\text{tot}}^\pm = \sum_k \bar{h}_k^\pm$ , interior (-) and exterior (+) to the element boundary being set  
 98 equal along the boundary of element  $n$ ,  $r_n = r_{n0}$ . Head matching along the circumference of  
 99 element 2 is expressed in terms of  $\bar{\Phi}$  as

$$\frac{1}{K_0} \left[ \bar{\Phi}_2^+ + \bar{\Phi}_1^+ + \bar{\Phi}_4 \right]_{r_{20}} = \frac{1}{K_2} \left[ \bar{\Phi}_2^- + \bar{\Phi}_3^+ \right]_{r_{20}}, \quad (7)$$

100 where the subscript indicates a local coordinate system, and the super-scripted sign indicates  
 101 the side of a two-sided element. Point source  $Q_5$  and the insides of circles 1 and 3 do not appear  
 102 in this expression, as they are neither immediately internal nor external to element 2. This con-  
 103 vention is used by other AEM applications that solve the modified Helmholtz equation [28, 19]  
 104 and is equivalent to the non-overlapping domain decomposition approach called substructuring  
 105 [29]; it allows regions with different coefficients in the governing equation to be matched, since  
 106 they cannot be combined by superposition.

107 Flux matching applies to the same elements as head matching and consists of setting

$$\mathbf{n}_n \cdot \bar{\mathbf{q}}_{\text{tot}}^+(r_{n0}) = \mathbf{n}_n \cdot \bar{\mathbf{q}}_{\text{tot}}^-(r_{n0}) \quad (8)$$

108 where  $\mathbf{n}_n$  is the unit boundary normal for element  $n$  and  $\bar{\mathbf{q}} = -\nabla \bar{\Phi}$  is the Darcy flux; the total  
 109 normal flux,  $\mathbf{n} \cdot \bar{\mathbf{q}}_{\text{tot}}^\pm = \sum_k \mathbf{n} \cdot \bar{\mathbf{q}}_k^\pm$ , is balanced along the boundary of element  $n$ . For element 2  
 110 in Figure 1, in terms of  $\bar{\Phi}$ , this yields

$$\left[ \frac{\partial \bar{\Phi}_2^+}{\partial r_2} + \frac{\partial \bar{\Phi}_1^+}{\partial r_1} J_{r_1 r_2} + \frac{\partial \bar{\Phi}_4^+}{\partial \theta_1} J_{\theta_1 r_2} + \frac{\partial \bar{\Phi}_4}{\partial r_4} J_{r_4 r_2} \right]_{r_{20}} = \left[ \frac{\partial \bar{\Phi}_2^-}{\partial r_2} + \frac{\partial \bar{\Phi}_3^+}{\partial r_3} J_{r_3 r_2} + \frac{\partial \bar{\Phi}_3^+}{\partial \theta_3} J_{\theta_3, r_2} \right]_{r_{20}}, \quad (9)$$

111 where  $J_{\theta_1 r_2} = \frac{\partial \theta_1}{\partial x} \frac{\partial x}{\partial r_2} + \frac{\partial \theta_1}{\partial y} \frac{\partial y}{\partial r_2}$  is a Jacobian relating derivatives in two coordinate systems. Each  
 112 of these coordinate derivatives in the Jacobian can be computed explicitly from the geometry of

113 the elements.  $\bar{\Phi}$  for each element is defined in terms of a local coordinate system (corresponding  
 114 to the one used in separation of variables); differentiation with respect to local coordinates  
 115 (e.g.,  $\partial\bar{\Phi}_2^+/\partial r_2$ ) leads to more concise expressions than working with a single set of coordinates  
 116 everywhere.

### 117 2.3. SOLUTION FOR COEFFICIENTS

118 The modified Helmholtz equation (3) involves 2 or 3 independent variables (depending on the  
 119 dimension,  $D$ ). The eigenfunction expansion solution is the tensor product of the solutions  
 120 obtained through separation of variables [3],

$$\bar{\Phi}_k^\pm(\mathbf{x}) = \prod_{i=1}^D \bar{\Phi}_k^\pm(x_i), \quad (10)$$

121 where  $\bar{\Phi}_k^\pm(x_i)$  is a sum of eigenfunctions for the coordinate  $x_i$  and element  $k$ . The orthogonal  
 122 eigenfunctions here are special functions (e.g., Bessel [30, Chap. 6–8] and Mathieu [31, Chap.  
 123 9] functions).  $\bar{\Phi}$  is expanded in eigenfunctions along element boundaries; the solution is then  
 124 computed on or away from the boundaries using the coefficients determined from the boundary  
 125 expansion. The second-order ordinary differential equations used here have solutions of the form,

$$\bar{\Phi}_k^\pm(x_i) = \sum_{j=0}^{N-1} a_j^{k\pm} \phi_j(x_i) + b_j^{k\pm} \psi_j(x_i) + R_N^k, \quad (11)$$

126 where  $\phi_j(x_i)$  and  $\psi_j(x_i)$  are the eigenfunctions associated with the  $j^{\text{th}}$  eigenvalue and coordinate  
 127  $x_i$ ;  $a_j^{k\pm}$  and  $b_j^{k\pm}$  are free coefficients [ $L^3$ ] to be determined for the  $\pm$  side of element  $k$ . The  
 128 residual,  $R_N$ , arises from truncating the infinite expansion. Upon recombination of the solutions  
 129 corresponding to the different coordinate variables (10) products of coefficients are consolidated.

130 Equations (10) and (11) constitute an exact expression for  $\bar{\Phi}_k^\pm$ , since  $R_N^k \rightarrow 0$  as  $N \rightarrow \infty$   
 131 in a least-squares sense [32] if the eigenfunctions form a complete set. Convergence is at least  
 132  $\mathcal{O}(N^{-2})$  for smooth functions with continuous first derivatives [3, Sect. 2.3]. The condition of  
 133 smoothness is not overly restrictive for physical problems. In cases where discontinuous functions  
 134 must be expanded (e.g., intersecting or touching elements), convergence will be degraded, but  
 135 the situation can often be improved with series transformation [33] or smoothing [34, Sect. 49]  
 136 techniques.

137 Elements either have specified strength ( $a_j^k$  and  $b_j^k$  are prescribed) or they have total head or  
 138 flux specified in a way which depends on the strength of other elements. LT-AEM requires three  
 139 steps to compute head or flux. The first step solves for the coefficients of the eigenfunctions using  
 140 boundary collocation, based on a desired arrangement of elements, source terms, and material  
 141 properties. The solutions to (11) that arise in the current coordinate system are substituted into  
 142 (10) at matching points along the element boundaries to obtain expressions for the coefficients  
 143 of the elements. In problems with multiple elements, the coefficients must be either estimated  
 144 iteratively (a fixed-point iteration over all elements) or using a direct matrix formulation. The  
 145 second step evaluates the solution at the desired  $\mathbf{x}$  and  $p$ , using the coefficients. Once the  
 146 Laplace-space solution and its derivatives are computed, the third step computes the time-  
 147 domain solution for head and flux at each location using a numerical inverse Laplace transform  
 148 algorithm.

### 149 2.4. LT-AEM IN RELATION TO AEM

150 Although conceptually LT-AEM is an application of AEM to (3), the implementation is different  
 151 in several respects. Since (3) contains  $p$ , which is complex, the special functions that satisfy (11)  
 152 have complex arguments or parameters. Although some inverse Laplace transform methods only

153 require real  $p$ , they are usually less successful at inverting discontinuous time behaviors (e.g., [35,  
154 Chap. 9] and [36, Chap. 19]), unless the calculations are performed using very high numerical  
155 precision [37].

156 Steady 2D AEM traditionally utilize the complex potential formulation,  $\Omega = \Phi + i\Psi$  (where  
157  $\Psi$  is a streamfunction), based on the Cauchy-Riemann relations. In LT-AEM both  $\bar{\Phi}$  and  $\bar{\Psi}$   
158 are complex, hence this convention is not applicable, although there are analogous Cauchy-  
159 Riemann expressions for the modified Helmholtz equation if  $\Phi$  and  $\Psi$  are real valued [23]. For  
160 steady flow  $\Psi$  coincides with particle traces, but in transient problems streamlines and pathlines  
161 are generally different.

162 For steady 2D AEM, an important distinction is made between elements which have an effect  
163 at “infinity” and those which do not (functions of  $\Omega$  with and without a branch cut) [12, Sect.  
164 19]. LT-AEM elements are derived considering that at finite time there is no effect at  $\infty$ , which  
165 simplifies derivation and implementation. In the limit as  $t \rightarrow \infty$  ( $p \rightarrow 0$ ), these elements would  
166 have effects at infinite distance (as  $p \rightarrow 0$ , (3) becomes the Laplace equation). Therefore, in  
167 LT-AEM there are no branch cuts to consider or far-field fixed heads that must be set to obtain  
168 a solution, as is required for several common elements in 2D steady-state AEM.

169 Lastly, LT-AEM can readily be modified to handle certain distributed source terms. Analo-  
170 gous source terms for  $\nabla^2\Phi = 0$  also lead to the Helmholtz equation [7, 19, 20], but would require  
171 a significant change in the solution approach. Leakage and transient effects must be dealt with  
172 approximately [18] or using area sources [15] in traditional AEM for the Laplace equation, but  
173 are readily handled with, or lead to, the Helmholtz equation.

### 174 3. LT-AEM Elements

#### 175 3.1. TAXONOMY

176 Two-dimensional LT-AEM elements can be categorized with respect to:

- 177 1. boundary condition and whether element coefficients are prescribed (i.e., “given” in AEM  
178 literature);
- 179 2. element geometry (e.g., line or area);
- 180 3. changes to source terms or constants in the governing equation (e.g., wave number or initial  
181 conditions);
- 182 4. element time behavior (e.g., constant, square wave, or pulse).

183 The free parameters for prescribed elements are independent of other elements in the system  
184 (e.g., a well with specified pumping rate). Circles, ellipses, and lines usually define regions of  
185 different aquifer parameters, and their coefficients must be determined at run-time. Variable  
186 time behavior for any type of element is handled in LT-AEM using Laplace-space convolution.

#### 187 3.2. BOUNDARY CONDITIONS

188 We use boundary condition matching to determine free coefficients; boundary conditions can  
189 be Dirichlet, Neumann, or of mixed type. Interface (i.e., matching or continuity) boundary con-  
190 ditions are posed along boundaries between regions defined by 2D elements. A mixed boundary  
191 condition along the circumference of an element is

$$\xi \nabla \bar{\Phi} \cdot \mathbf{n} + \zeta \bar{\Phi} = \bar{F}(s, p), \quad (12)$$

192 where  $s$  is arc length along the boundary. Setting  $\xi = 0$ ,  $\zeta = 1$  leaves a Dirichlet boundary con-  
193 dition;  $\bar{F}_D(s, p) = K\bar{h}_{BC}(s, p)$  is the transformed head along the circumference of the element.

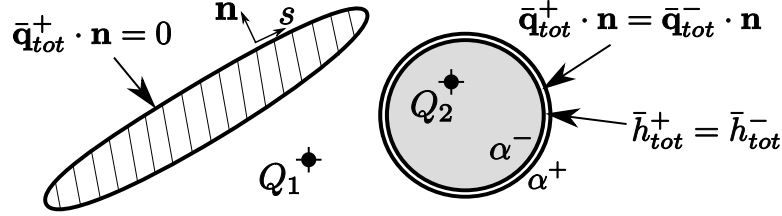


Figure 2. Example with no-flow ellipse, prescribed point sources and circular matching element with different  $\alpha$  inside and out (+ and - parts of matching element offset for clarity).

194 With  $\zeta = 0$ ,  $\xi = 1$ , (12) becomes a Neumann boundary condition; now  $\bar{F}_N(s, p) = \bar{q}_{BC}(s, p)$  is  
 195 the transformed normal flux on the element boundary.

196 Interface boundary conditions are associated with a two-sided element (see circle in Figure  
 197 2); we relate the Neumann and Dirichlet boundary conditions on each side, setting  $\bar{F}_N^+(s, p) =$   
 198  $\bar{F}_N^-(s, p)$  and  $(K^-/K^+)\bar{F}_D^+(s, p) = \bar{F}_D^-(s, p)$ , which enforce (6) and (8).

199 We can specify both a Dirichlet and a Neumann condition along the boundary for an elliptic  
 200 differential equation because we do not specify a value, but only indicate equality of the inside  
 201 and outside. Elements that are not interface conditions have their boundary conditions specified  
 202 in terms of total discharge potential (6) or normal flux, (8); if there are at least two elements,  
 203 their strengths must be determined simultaneously.

204 To determine element coefficients,  $M$  matching points are chosen along the element bound-  
 205 aries, creating a system of  $2M$  equations ( $M$  normal flux  $+M$  head), for the  $2N$  unknowns.  
 206 We use overspecification [38]; by choosing  $2M \geq 2N$  the system of equations is solved in a  
 207 least-squares sense. Overspecification often produces a smoother solution than  $2M = 2N$  does,  
 208 and for the same  $M$ ,  $N$  is smaller (i.e., the solution does not require the  $2M - 2N$  highest order  
 209 basis functions). For these reasons it is utilized in the LT-AEM. We use QR decomposition (as  
 210 done in the LAPACK [39] routine ZGELSS) to solve the least-squares problem, rather than  
 211 posing the traditional normal equations (e.g., [40, Sect. 5.3] and [41, Chap. 19]).

### 212 3.3. GEOMETRIC CONSIDERATIONS

213 Table I categorizes elements related to Helmholtz-separable 2D coordinates. Elliptical coordi-  
 214 nates are the most general 2D coordinates; polar, parabolic, and Cartesian coordinates can  
 215 be obtained by moving the elliptical foci together or moving one or both of the foci to  $\infty$ ,  
 216 respectively. In 2D, singular elements are sources or sinks, while areas are defined by finite  
 boundaries or infinite lines.

Table I. Helmholtz-separable 2D coordinate systems (e.g., [42], [43, Chap. 1], and [32, Sect. 5.3])

coordinate system	finite boundary	singular element	infinite boundary	modified Helmholtz special functions
Cartesian	<i>none</i>	$\infty$ line	$\infty$ line	exponential
polar (circular)	circle	point	ray	modified Bessel
elliptical	ellipse	line segment	hyperbola	modified Mathieu
parabolic	<i>none</i>	semi- $\infty$ line	parabola	parabolic cylinder

217

### 218 3.4. SOURCE TERMS

219 Individual elements or entire domains can be governed by differential equations other than (3);  
 220 they can be completely different (e.g., aLplace's equation) or only differ by material properties



221 or the presence of source terms. Source terms can be either homogeneous (functions of  $\bar{\Phi}$ ) or  
 222 inhomogeneous (a Poisson term). Homogeneous LT-AEM area sources can be handled without  
 223 modification to the solution process, since (3) contains this type of term, additional terms only  
 224 change the definition of  $\kappa^2$ , the wave number. Poisson terms (including  $\Phi_0$  in (2)) must be  
 225 expressed in terms of a particular solution.

### 226 3.4.1. Homogeneous leaky aquifer source term

227 Homogeneous source terms arise from effects that are proportional to changes in head or draw-  
 228 down in the aquifer. For example, transient leakage from adjacent aquitards, delayed yield in  
 229 unconfined systems, and dual-domain behavior all lead to homogeneous source terms [4, Sect.  
 230 4.2]. Because the 2D LT-AEM does not represent the third dimension explicitly, Neumann  
 231 boundary conditions with respect to the third dimension (e.g.,  $\partial\bar{\Phi}/\partial z|_{z=0}$ ) must be represented  
 232 as distributed source terms.

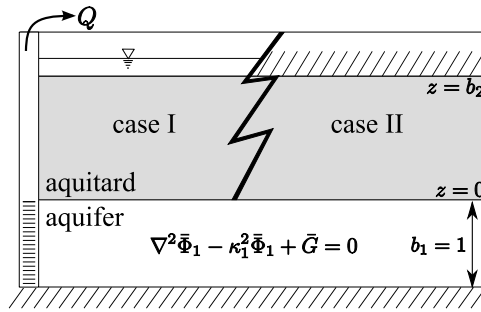


Figure 3. Leaky system diagram

233 Leakage from an adjacent unpumped aquitard leads to a homogeneous distributed source  
 234 in 2D. We adapt Hantush's modified leaky system [44] to LT-AEM (see Figure 3). Beginning  
 235 with (1) but considering a non-zero source term,  $G$ , when expressing the system in terms of  $\bar{\Phi}$ ,  
 236 and taking the Laplace transform leads to

$$\nabla^2 \bar{\Phi}_1 - \kappa_1^2 \bar{\Phi}_1 + \bar{G} = 0, \quad (13)$$

237 where subscript 1 indicates the aquifer and 2 the aquitard. Assuming vertical flow in the overly-  
 238 ing aquitard (a common assumption when  $K_1 \gg K_2$ ), (3) simplifies to an ordinary differential  
 239 equation for  $\bar{\Phi}_2$ ,

$$\frac{d^2 \bar{\Phi}_2}{dz^2} - \kappa_2^2 \bar{\Phi}_2 = 0, \quad (14)$$

240 where the initial value of  $\bar{\Phi}_2$  is zero. The head-matching boundary condition at the aquifer-  
 241 aquitard interface ( $z = 0$ ) is  $\bar{\Phi}_2 = K_2 \bar{\Phi}_1 / K_1$ , and at the top of the aquitard ( $z = b_2$ ) there is a  
 242 no-drawdown condition,  $\bar{\Phi}_2 = 0$  (see case I of Figure 3). The solution to (14) that satisfies both  
 243 conditions is

$$\bar{\Phi}_2(z) = \frac{K_2 \bar{\Phi}_1}{K_1} [\cosh \kappa_2 z - \coth \kappa_2 b_2 \sinh \kappa_2 z]. \quad (15)$$

244 Differentiating (15) and evaluating it at  $z = 0$  gives the vertical flux from the aquitard at the  
 245 interface,

$$\bar{G} = \frac{1}{b_1} \left[ \frac{\partial \bar{\Phi}_2}{\partial z} \right]_{z=0}; \quad (16)$$

246 when this is substituted into (13), the governing equation in the aquifer becomes

$$\nabla^2 \bar{\Phi}_1 - \left[ \kappa_1^2 + \kappa_2 \frac{K_2}{b_1 K_1} \coth \kappa_2 b_2 \right] \bar{\Phi}_1 = 0. \quad (17)$$

247 This can be solved using the same solution techniques used for (3) because the new terms in (17)  
 248 are all constants that redefine the wave number. Since the governing equation in the aquitard  
 is linear with homogeneous initial and boundary conditions, superposition is valid.

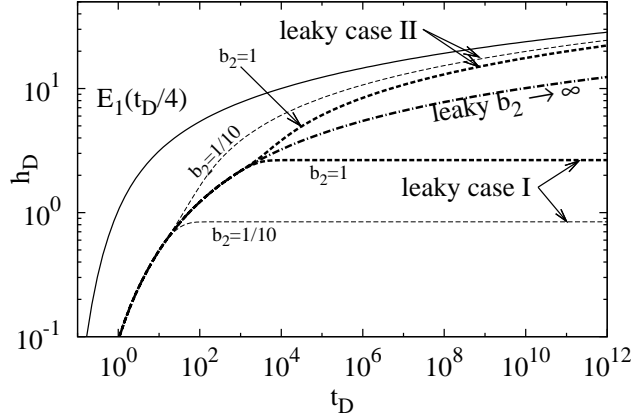


Figure 4. Leaky response at  $r = 1$  due to point source (18), comparing results for different aquitard boundary conditions and aquitard thicknesses with the non-leaky  $E_1$  solution;  $S_{s2}/S_{s1} = 100$ ,  $K_1/K_2 = 5$ .

249 Figures 4, 5, and 6 show effects due to a constant strength finite-radius well source (e.g., [6]  
 250 and [45, Sect. 4.3.2], which for (3) is

$$\bar{\Phi}_{\text{well}}(r) = \frac{Q}{2\pi b_1 p} \frac{K_0(r\kappa)}{\kappa r_w K_1(r_w \kappa)}, \quad (18)$$

252 where  $K_0$  and  $K_1$  are modified Bessel functions (see [27, Sect. 9.6] or [30, Sect. 7.2] for properties),  
 253  $r_w$  is the pumping well radius [ $L$ ], and  $Q$  is the pumping rate [ $L^3/T$ ]. to exploit axial symmetry,  
 254 plots show dimensionless results;  $t_D = tK_1/(S_{s1}r^2)$  is dimensionless time and  $s_D = 4\pi|\Phi - \Phi_0|/Q$   
 255 is dimensionless drawdown. The curve labeled  $E_1(t_D/4)$  represents the non-leaky Theis solution  
 256 [46], an exponential integral (see [27, Chap. 5] or [30, Sect. 3.4] for properties). The well solution  
 257 (18) to (17) produces the flattening curves in Figure 4.

258 A similar procedure is used to develop a leaky solution with a different aquitard boundary  
 259 condition; the equation for a no-flow boundary condition at  $z = b_2$  is (case II, the upwardly-  
 260 deviating curves in Figure 4)

$$\nabla^2 \bar{\Phi}_1 - \left[ \kappa_1^2 + \kappa_2 \frac{K_2}{b_1 K_1} \tanh \kappa_2 b_2 \right] \bar{\Phi}_1 = 0. \quad (19)$$

261 For the thick aquitard case ( $b_2 \rightarrow \infty$ ),  $\coth \kappa_2 b_2$  in (17) and  $\tanh \kappa_2 b_2$  in (19) simplify to unity  
 262 (the middle leaky curve in Figure 4). The effects of the boundary condition at  $z = b_2$  are only  
 263 observed at later time when the three curves separate (the thin curves in Figure 4 represent an  
 264 aquitard 1/10 as thick as the heavy curves — they deviate at an earlier time). The effects of two  
 265 aquitards (above and below) can be included, as done by Hantush [44]. The second aquitard  
 266 adds another term, analogous to those in (17) and (19).

### 267 3.4.2. Homogeneous source due to extended form of Darcy's law

268 Higher-order time derivatives in the governing time-domain equation (representing inertia) also  
 269 lead to a homogeneous source term in the Laplace-domain. The effect of not considering this  
 270 inertia term, in situations where it may be significant (e.g., the coarse gravel-packed region  
 271 surrounding a pumping well), may lead to slight over-estimation of storage parameters with  
 272 diffusion models. Consider the more complete transient form of Darcy's law (averaged from, or



273 through analogy with, the Navier-Stokes equations (e.g., [47, Sect. 5.10.6] and [48, Sect. 1.5]),  
 274 given as

$$\mathbf{q} = - \left( \nabla \Phi + \tau \frac{\partial \mathbf{q}}{\partial t} \right), \quad (20)$$

where  $\tau$  is the relaxation parameter [T], a property related to the time it takes the system

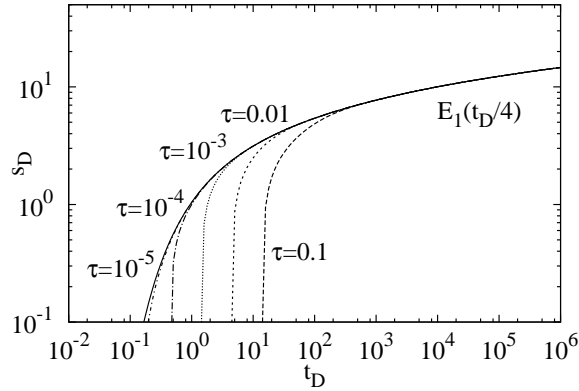


Figure 5. Time-drawdown at  $r = 1$  for point source (18) considering inertia effects.

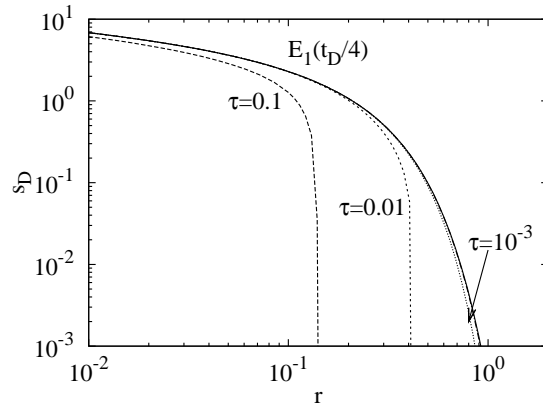


Figure 6. Distance-drawdown at  $t = 0.01$  for point source (18) considering inertia effects.

275 to become diffusion-dominated. Typically  $\tau$  is small and the time derivative term is neglected.  
 276 L fqvist and Reh binder [49] define  $\tau = K/(ng)$ , where  $n$  is dimensionless porosity and  $g$  is the  
 277 acceleration due to gravity [ $L/T^2$ ]. Combining the Laplace-space mass-conservation equation,  
 278

$$-\nabla \cdot \bar{\mathbf{q}} - \kappa^2 \bar{\Phi} = 0, \quad (21)$$

279 with the Laplace transform of (20), the governing equation becomes

$$\nabla \cdot \left[ \frac{1}{1 + \tau p} \nabla \bar{\Phi} \right] - \kappa^2 \bar{\Phi} = 0, \quad (22)$$

280 assuming initial head and flux are zero. This can be put into the form

$$\nabla^2 \bar{\Phi} - \left[ \kappa^2 + \tau \frac{p^2}{\alpha} \right] \bar{\Phi} = 0, \quad (23)$$

281 which is again similar to (3), but with an additional  $p^2$  term in the wave number. Equation (23)  
 282 can be solved for a point source by redefining the wave number in (18) (see Figures 5 and 6).

283 Equation 23 is the transformed damped wave equation, a more general form of the diffusion  
 284 equation [25, Chap. 8]. For problems governed by the wave equation, pulses always propagate at  
 285 finite speed (e.g., see steep leading edge of  $s_D$  surface in Figure 6), while the diffusion equation  
 286 allows changes to propagate at infinite speed [50, Sect. 1.2.1]. For example,  $s_D = E_1(t_D/4)$   
 287 (Theis [46] solution) produces non-zero drawdown at every  $r$  for  $t > 0$ ; as  $r \rightarrow \infty$   $s_D \rightarrow 0$ , so  
 288 this discrepancy is usually tolerated. In the damped wave equation  $\tau$  is inversely proportional  
 289 to the maximum propagation velocity squared; as  $\tau \rightarrow 0$ , the maximum velocity  $\rightarrow \infty$ , and the  
 290 damped wave equation becomes the diffusion equation.

291 The two distributed source terms discussed in this section are illustrated using (18), but  
 292 are easily extended to other elements [4, Sect. 4.2]. An elliptical line or area source [22] with  
 293 a wave number corresponding to a leaky problem is a trivial extension to the existing line or  
 294 area element, thus analytic solutions to other geometries and superpositions thereof are readily  
 295 found.

### 296 3.4.3. *Inhomogeneous source terms*

297 Area sources can be used to represent constant recharge or discharge, or variable recharge where  
 298 the source term is not proportional to aquifer drawdown. For circular elements, Kuhlman and  
 299 Neuman [22] showed that  $\Phi_0 \neq 0$  can be represented as impulse area sources by decomposing  
 300 the solution to the inhomogeneous governing equation into a homogeneous and a particular  
 301 solution [12, Sect. 37].

302 The particular solution for an initial condition that is linear or constant in space can be  
 303 found by inspection, since the Laplacian of this type of function has zero contribution to the  
 304 particular solution. Inhomogeneous terms with more general spatial behavior may be computed  
 305 numerically using area integration of the Green's function, through variation of parameters  
 306 using known eigenfunctions, or derived as area sources in general functional forms (e.g., 2D  
 307 multi-quadric surfaces [51]).

## 308 4. Elliptical elements

309 Circular LT-AEM elements are given by Furman and Neuman [6], while elliptical elements  
 310 are derived here using an analogous procedure [4, Sect. 3.2]. Bakker [28, 52] and Bakker and  
 311 Nieber [8] derived elliptical AEM elements for the modified Helmholtz equation. A significant  
 312 difference between their elliptical AEM solutions and that given here is the presence of the  
 313 complex Laplace parameter,  $p$ , which becomes large at small time; this is because  $p$  and  $t$   
 314 are multiplicative arguments to the exponential in the definition of the Laplace transform (e.g., [34,  
 Sect. 4.24] and [26, Chap. 7]).

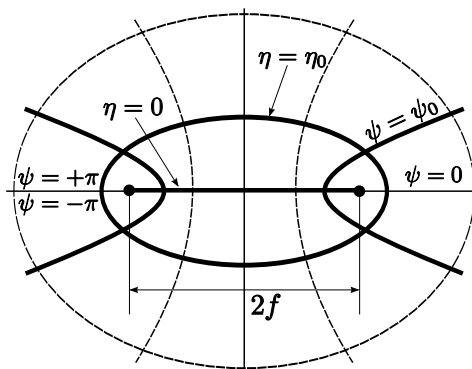


Figure 7. Components of elliptical coordinates  $(\eta, \psi)$ ;  $f$  is semi-focal distance.

315 Elliptical coordinates (see Figure 7) are defined as  $x = f \cosh \eta \cos \psi$  and  $y = f \sinh \eta \sin \psi$ ,  
 316 where  $(\eta, \psi)$  are dimensionless elliptical coordinates and  $f$  is the semi-focal length  $[L]$ . The  
 317

318 transforms are given succinctly in terms of a conformal map; when  $z = x + iy$  and  $\zeta = \eta + i\psi$ ,  
 319 the forward transform is  $z = f \cosh \zeta$  and the backward transform is  $\zeta = \operatorname{arccosh} z/f$ . The  
 320 multi-valued complex inverse hyperbolic cosine can be expressed as a single-valued function [53]  
 321 in the form

$$\zeta = \begin{cases} \ln \left( z/f + \sqrt{(z/f)^2 - 1} \right) & x > 0, \\ \ln \left( z/f - \sqrt{(z/f)^2 - 1} \right) & x \leq 0. \end{cases} \quad (24)$$

322 The modified Helmholtz equation (3) in elliptical coordinates (e.g., [31, Chap. 9], [43, p. 17],  
 323 [32, p. 1407]) is

$$\frac{2}{f^2 [\cosh 2\eta - \cos 2\psi]} \left[ \frac{\partial^2 \bar{\Phi}}{\partial \eta^2} + \frac{\partial^2 \bar{\Phi}}{\partial \psi^2} \right] - \kappa^2 \bar{\Phi} = 0, \quad (25)$$

324 with the condition that  $\bar{\Phi}(\psi) = \bar{\Phi}(\psi + 2\pi)$ . Upon substitution of the form  $\bar{\Phi}(\eta, \psi) = H(\eta)\Psi(\psi)$ ,  
 325 (25) can be separated into two ordinary differential equations,

$$\frac{d^2 \Psi}{d\psi^2} + (\omega - 2q \cos 2\psi) \Psi = 0, \quad (26a)$$

326

$$\frac{d^2 H}{d\eta^2} - (\omega - 2q \cosh 2\eta) H = 0, \quad (26b)$$

327 where  $\omega$  is a separation constant (Mathieu characteristic number  $a$  or  $b$  in Mathieu function  
 328 literature) and  $q = -f^2 \kappa^2 / 4$  is the Mathieu parameter. These are the angular (26a) and radial  
 329 (26b) Mathieu equations. The parameter  $q$  is specified through the aquifer properties, element  
 330 geometry, and  $p$ , while  $\omega$  is determined to make the solution to (26a) periodic on  $\pi \leq \psi < -\pi$ .  
 331 The special functions that are solutions to (26a) and (26b) are Mathieu functions; see [54, 8, 55]  
 332 for characteristic functional plots. Solutions to (25) for  $\Re(q) < 0$  are

$$\bar{\Phi}_e^+(\eta, \psi) = \sum_{n=0}^{\infty} a_n \operatorname{Ke}_n(\eta; -q) \operatorname{ce}_n(\psi; -q) + \sum_{n=1}^{\infty} b_n \operatorname{Ko}_n(\eta; -q) \operatorname{se}_n(\psi; -q), \quad (27a)$$

333

$$\bar{\Phi}_e^-(\eta, \psi) = \sum_{n=0}^{\infty} c_n \operatorname{Ie}_n(\eta; -q) \operatorname{ce}_n(\psi; -q) + \sum_{n=1}^{\infty} d_n \operatorname{Io}_n(\eta; -q) \operatorname{se}_n(\psi; -q), \quad (27b)$$

334 where  $a_n$ ,  $b_n$ ,  $c_n$  and  $d_n$  are the coefficients to be determined,  $\operatorname{Ie}_n$ ,  $\operatorname{Io}_n$ ,  $\operatorname{Ke}_n$ , and  $\operatorname{Ko}_n$  are the  
 335 even (e) and odd (o) radial Mathieu function of first and second kind, and  $\operatorname{ce}_n$  and  $\operatorname{se}_n$  are  
 336 the even (cosine-elliptic) and odd (sine-elliptic) first-kind angular Mathieu function. Equation  
 337 27a only contains the second-kind radial Mathieu functions ( $\operatorname{Ke}_n$ ,  $\operatorname{Ko}_n$ ) which are finite as  
 338  $\eta \rightarrow \infty$ . Similarly, (27b) only contains the first-kind radial Mathieu function ( $\operatorname{Ie}_n$ ,  $\operatorname{Io}_n$ ) that has  
 339 continuous value and slope across the focal line,  $\eta = 0$ . Because  $\Re(q) < 0$  these are modified  
 340 Mathieu functions.

341 To simplify the expression for head matching (6) on the boundary of the ellipse, the radial  
 342 Mathieu functions are normalized, resulting in

$$\bar{\Phi}_e^+(\eta \geq \eta_0, \psi) \approx \sum_{n=0}^{N-1} a_n \frac{\operatorname{Ke}_n(\eta; -q^+)}{\operatorname{Ke}_n(\eta_0; -q^+)} \operatorname{ce}_n(\psi; -q^+) + \sum_{n=1}^{N-1} b_n \frac{\operatorname{Ko}_n(\eta; -q^+)}{\operatorname{Ko}_n(\eta_0; -q^+)} \operatorname{se}_n(\psi; -q^+), \quad (28a)$$

343

$$\bar{\Phi}_e^-(\eta \leq \eta_0, \psi) \approx \sum_{n=0}^{N-1} c_n \frac{\operatorname{Ie}_n(\eta; -q^-)}{\operatorname{Ie}_n(\eta_0; -q^-)} \operatorname{ce}_n(\psi; -q^-) + \sum_{n=1}^{N-1} d_n \frac{\operatorname{Io}_n(\eta; -q^-)}{\operatorname{Io}_n(\eta_0; -q^-)} \operatorname{se}_n(\psi; -q^-), \quad (28b)$$

344 where the infinite sum has been truncated and the  $\pm$  superscripts on  $q$  indicate whether it in-  
 345 volves aquifer parameters from inside ( $-$ ) or outside ( $+$ ) the ellipse  $\eta = \eta_0$ . In polar coordinates,

346 a similar set of expressions is derived [16, 6]; they are

$$\bar{\Phi}_c^+(r \geq r_0, \theta) \approx \gamma_0 \frac{K_0(r\kappa^+)}{K_0(r_0\kappa^+)} + \sum_{n=1}^{N-1} \frac{K_n(r\kappa^+)}{K_n(r_0\kappa^+)} [\gamma_n \cos(n\theta) + \delta_n \sin(n\theta)]. \quad (29)$$

347 The first difference between (29) and (28a) is the “even” and “odd” radial functions in elliptical  
 348 coordinates. A second difference is the appearance of both an argument ( $\eta$  or  $\psi$ ) and a parameter,  
 349  $q^\pm$ , in (28a) and (28b). Thirdly, both radial and angular Mathieu functions depend on the  
 350 coefficients of the partial differential equation (through  $q$ ), while sine and cosine in (29) do not.

#### 351 4.1. LINE SOURCE

352 An expression for a constant flux line source (along  $y = 0$ , from  $-f \leq x \leq f$ ) is obtained  
 353 from (27a), using only  $ce_{2n}(\psi; -q)$  due to symmetry. To simplify flux matching (8) we normalize  
 354 by the radial Mathieu function derivative,  $Ke'_{2n}(0; -q)$ , giving

$$\bar{\Phi}_{\text{line}}(\eta, \psi) = \sum_{n=0}^{\infty} \beta_{2n} ce_{2n}(\psi; -q) \frac{Ke_{2n}(\eta; -q)}{Ke'_{2n}(0; -q)}, \quad (30)$$

355 where  $\beta_{2n}$  are the coefficients to be determined. The boundary condition for a specified flux line  
 356 element in elliptical coordinates is

$$\bar{q}_{\text{BC}} = \bar{g}(p) \frac{\bar{\lambda}}{2f} = - \frac{1}{f \sqrt{\frac{1}{2} (\cosh 2\eta - \cos 2\psi)}} \left. \frac{\partial \bar{\Phi}_{\text{line}}}{\partial \eta} \right|_{\eta=\eta_0}, \quad (31)$$

357 where  $\bar{\lambda}$  is the transformed constant flowrate [ $L^3$ ],  $2f$  is the length of the line segment, and  
 358  $\bar{q}_{\text{BC}}$  is the normal flux [ $L$ ] due to the line source. The metric coefficient in the denominator is  
 359 required to preserve the correct dimensions [32, Sect. 1.3]. Differentiating (30) with respect to  
 360  $\eta$ , evaluating it at  $\eta = 0$ , and using orthogonality over  $0 < \psi < \pi$  gives

$$-\bar{g}(p) \frac{\bar{\lambda}}{2} \int_0^\pi \sin \psi ce_{2m}^*(\psi; -q) d\psi = \sum_{n=0}^{\infty} \beta_{2n} \int_0^\pi ce_{2n}(\psi; -q) ce_{2m}^*(\psi; -q) d\psi, \quad (32)$$

361 where  $ce_{2m}(\psi; -q)$  has period  $\pi$  and  $*$  is complex conjugate. Due to the orthogonality of the  
 362 angular Mathieu functions, the integral on the right in (32) is 0 for  $m \neq n$  and is defined as  $\pi/2$   
 363 for  $m = n$  [31, Sect. 2.19], reducing the infinite sum to the  $2m^{\text{th}}$  term. The expression for the  
 364 coefficients is

$$\beta_{2m} = -\bar{g}(p) \frac{\bar{\lambda}}{\pi} \int_0^\pi ce_{2m}^*(\psi; -q) \sin \psi d\psi. \quad (33)$$

365 Expanding  $ce_{2m}^*$  in terms of its defining infinite cosine series (A1a), and evaluating the resulting  
 366 integral leaves

$$\beta_{2m} = \bar{g}(p) \frac{2\bar{\lambda}}{\pi} (-1)^{m+1} \left[ \sum_{r=0}^{\infty} (-1)^r \frac{A_{2r}^{(2m)*}}{1 - (2r)^2} \right], \quad (34)$$

367 where  $A_{2r}^{(2m)}$  is a matrix of Mathieu coefficients (see Appendix A). The terms in the infinite sum  
 368 quickly become small as  $r$  increases and the largest magnitude terms in  $A_{2r}^{(2m)}$  occur surrounding  
 369 the diagonal  $r = m$  (as  $q \rightarrow 0$ ,  $A_{2r}^{(2m)}$  becomes a diagonal matrix). Substituting (34) back into  
 370 (30) gives the final expression for a constant strength passive line source as

$$\bar{\Phi}_{\text{line}}(\eta, \psi) = \bar{g}(p) \frac{4\bar{\lambda}}{\pi} \sum_{n=0}^{\infty} (-1)^{n+1} \left[ \sum_{r=0}^{\infty} (-1)^r \frac{A_{2r}^{(2n)*}}{1 - (2r)^2} \right] ce_{2n}(\psi; -q) \frac{Ke_{2n}(\eta; -q)}{Ke'_{2n}(0; -q)}. \quad (35)$$

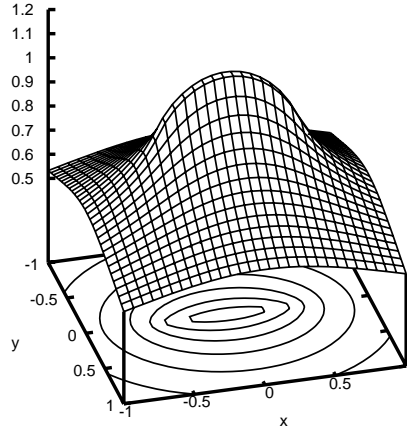


Figure 8. Constant strength line source solution for  $f = 0.5$ ,  $Q = 1$ ,  $\alpha = 5.0 \times 10^4$ ,  $t = 0.0125$ ;  $h$  contour interval is 0.1

371 This formulation of the transient line source is valid for any length line source and can take on  
 372 different time behaviors through convolution with various  $\bar{g}(p)$ . Figure 8 illustrates the solution  
 373 for  $\bar{g}(p) = 1/p$  (a constant strength starting at  $t = 0$ ), using  $M = 20$  and an infinite matrix for  
 374 the Mathieu functions truncated at 42 terms. Tranter [56] derived a real-valued Mathieu function  
 375 solution for the case of an ellipse with a Dirichlet boundary condition. Kucûk and Brigham [57]  
 376 applied Tranter's solution to flow in anisotropic petroleum reservoirs, and Riley [58] derived  
 377 expression for flow in a petroleum reservoir to a linear crack. Kuhlman and Warrick [20] derived  
 378 a Mathieu function solution for linearized infiltration from an ellipse. Morse and Feshbach [32,  
 379 p. 1419–1425] give a solution in terms of Mathieu functions for a Neumann boundary condition  
 380 similar to flow through a slot, with real and positive  $q$ , while Erricolo [59] shows how these types  
 381 of series can be accelerated to minimize the number of Mathieu function evaluations.

382 The flux normal to the line source at  $\eta = 0$ , illustrated in Figure 8, is compared to the  
 383 true boundary condition in Figure 9 for increasing numbers of terms in the Mathieu function  
 384 expansion. The numerically-integrated average error, along the boundary of the element, is 0.011  
 385 for  $N = 4$  and reduces to  $-3.6 \times 10^{-3}$  for  $N = 12$ ; the average error decreases slowly beyond  
 386 that as more terms are added. The solution converges slowest at the ends of the interval, where  
 387 the even function  $ce_{2n}(\psi)$  must force the flux to zero.

388 An ellipse or line element expressed in elliptical coordinates using Mathieu functions is useful  
 389 as an LT-AEM element with the coefficients of (27a) determined at run time or as an element  
 390 for the special case of strength constant in space (35). Using approximate methods, rather than  
 391 the appropriate eigenfunctions, may be better suited for intersecting line elements; similar to  
 392 those in [28], but using an approximation can accommodate large  $p$  values accurately.

393

## 5. Numerical Inverse Laplace Transform

394 Complex contour integration techniques could be used to analytically compute the time domain  
 395 solution from the Mellin contour integral (e.g., [21, Sect. 66] and [45, Sect. 3.2]), defined as

$$\Phi(\mathbf{x}, t) = \mathcal{L}^{-1} \{ \bar{\Phi}(\mathbf{x}, p) \} = \frac{1}{i2\pi} \int_{\sigma_0 - i\infty}^{\sigma_0 + i\infty} \bar{\Phi}(\mathbf{x}, p) e^{pt} dp \quad (36)$$

396 where  $\sigma_0 \geq 0$  is larger than the real part of the right-most singularity in  $\bar{\Phi}(\mathbf{x}, p)$ . Analytic  
 397 inversion techniques (e.g., method of residues) are very problem-specific and may only yield  
 398 a solution in the form of a slowly converging infinite series; using a numerical  $\mathcal{L}^{-1}$  allows

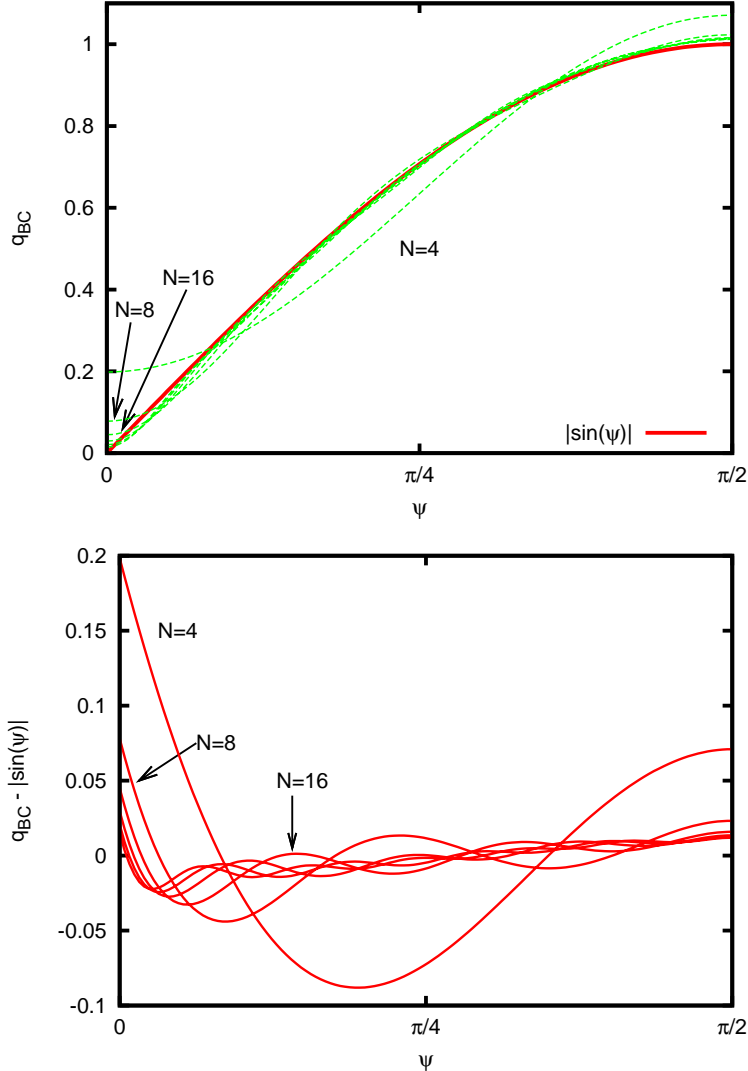


Figure 9. Flux boundary condition and error in Mathieu function expansion for line source in Figure 8.

399 flexibility and generality. See [35, Chap. 9], and the references therein, for general reviews and  
 400 comparisons of popular numerical numerical inverse Laplace transform algorithms; Kuhlman  
 401 [4, Chap. 5] discusses the details related to several alternative inverse methods in the context  
 402 of the LT-AEM.

403 A set of LT-AEM solutions are computed for required values of  $p$ , whose optimum values  
 404 depend on the algorithm being used. The time-domain solution is then approximated from this  
 405 set using a numerical inverse Laplace transform algorithm. Furman and Neuman [6] utilized the  
 406 doubly-accelerated Fourier series approach of de Hoog, et al. [60], but no method is universally  
 407 best. The Fourier series method can accurately invert an LT-AEM solution over a log-cycle of  
 408  $t$  values for a set of  $p$  optimized for  $t_{\max}$  (the largest  $t$  desired). The unaccelerated form of the  
 409 Fourier series algorithm is [36, Chap. 19],

$$\Phi(t) \approx \frac{e^{\sigma t}}{T} \sum_{k=0}^{2M'} \Re \left[ \bar{\Phi} \left( \sigma + \frac{i\pi k}{T} \right) \exp \left( \frac{i\pi k t}{T} \right) \right], \quad (37)$$

410 where  $T$  is a scaling parameter (typically  $2t_{\max}$ ), the first and last terms in the summation are  
 411 halved, and  $\sigma$  depends on the locations of the singularities in  $\bar{\Phi}$ . The argument of  $\bar{\Phi}$ , the results













